Biochar

ORIGINAL RESEARCH

Open Access

Preparation and characterization of MgO hybrid biochar and its mechanism for high efficient recovery of phosphorus from aqueous media

Yueru Fang[1], Amjad Ali[2], Yuxi Gao[1], Peng Zhao[1], Ronghua Li[1*], Xianxian Li[1], Junxi Liu[1], Yuan Luo[1], Yaru Peng[1], Hailong Wang[3], Hongbin Liu[4], Zengqiang Zhang[1] and Junting Pan[4*]

Abstract

Conversion of organic waste into engineered metal-biochar composite is an effective way of enhancing biochar's efficiency for adsorptive capture of phosphorus (P) from aqueous media. Thus, various strategies have been created for the production of metal-biochar composites; however, the complex preparation steps, high-cost metal salt reagent application, or extreme process equipment requirements involved in those strategies limited the large-scale production of metal-biochar composites. In this study, a novel biochar composite rich in magnesium oxides (MFBC) was directly produced through co-pyrolysis of magnesite with food waste; the product, MFBC was used to adsorptively capture P from solution and bio-liquid wastewater. The results showed that compared to the pristine food waste biochar, MFBC was a uniformly hybrid MgO biochar composite with a P capture capacity of 523.91 mg/g. The capture of P by MFBC was fitted using the Langmuir and pseudo-first-order kinetic models. The P adsorptive capture was controlled by $MgHPO_4$ formation and electrostatic attraction, which was affected by the coexisting F^- and CO_3^{2-} ions. MFBC could recover more than 98% of P from the solution and bio-liquid wastewater. Although the P-adsorbed MFBC showed very limited reusability but it can be substituted for phosphate fertiliser in agricultural practices. This study provided an innovative technology for preparing MgO-biochar composite against P recovery from aqueous media, and also highlighted high-value-added approaches for resource utilization of bio-liquid wastewater and food waste.

Highlights

- Co-pyrolysis of magnesite with food waste generated MgO hybrid biochar composite.
- MgO hybrid biochar showed a high phosphorus recovery capacity (523.9 mg/g).
- Phosphorus recovery was controlled by $MgHPO_4$ formation and electrostatic attraction.
- MgO hybrid biochar recovered > 98% of P from solution and bio-liquid wastewater.
- Recovered phosphorus is a slow-release fertilizer available for agriculture use.

*Correspondence: rh.lee@nwsuaf.edu.cn; panjunting@caas.cn

[1] College of Natural Resources and Environment, Northwest A&F University, Yangling, Xianyang 712100, Shaanxi, China
[4] Institute of Agricultural Resources and Regional Planning, Chinese Academy of Agricultural Sciences, Beijing 100081, China
Full list of author information is available at the end of the article

Keywords: Biochar, Bio-liquid wastewater, Fertiliser, Magnesite, Phosphorus recovery

Graphical Abstract

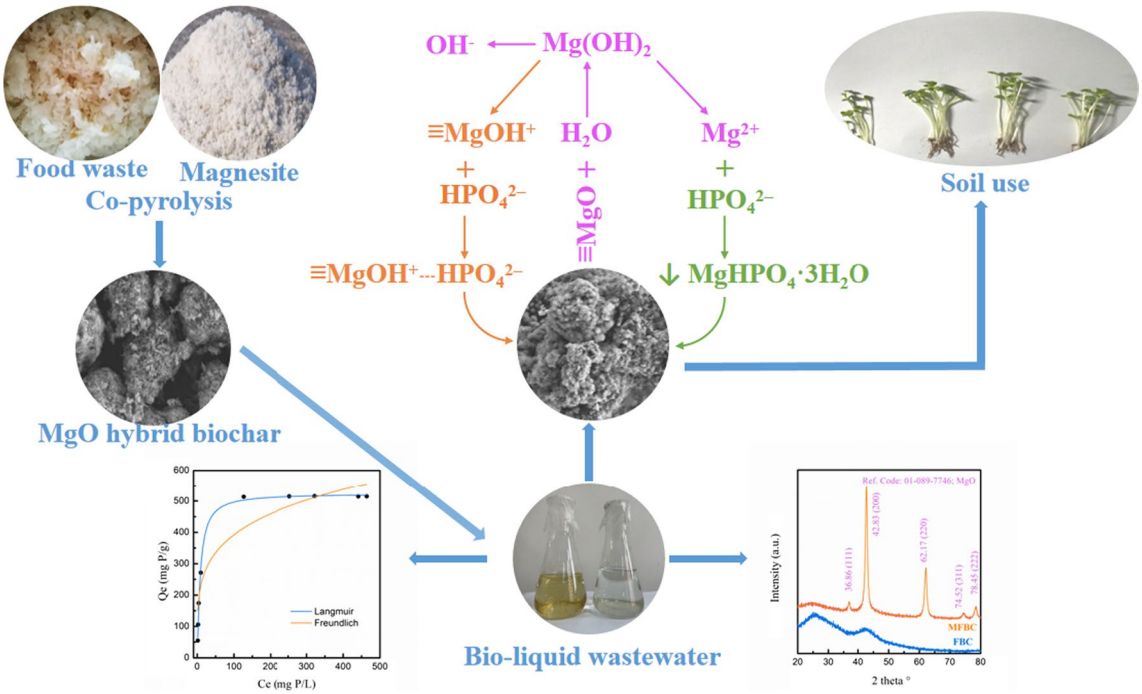

1 Introduction

Phosphorus (P) is an important plant nutrient, which is also a non-renewable resource (Fang et al. 2021). In agricultural production, it is necessary to supplement a large amount of P fertiliser for crop growth (Xie et al. 2021). With the rapid development of large-scale livestock and poultry farming, large amounts of bio-liquid wastewater were produced accordingly. It was confirmed that P emissions from livestock farming accounted for 56% of total P emissions from agricultural sources in China (Fan et al. 2020a, b). However, according to the US Geological Survey, the static utilisation period of China's P reserves is only 37 years (Fang et al. 2021). Therefore, recovery of P from P-rich water bodies, including bio-liquid wastewater, is an important initiative for alleviating the P resource crisis.

Among the various effective techniques used for recovering P from water, the adsorption method is considered one of the most effective and flexible measures in use (Li et al. 2018a). Accordingly, the production of new low-cost adsorbents from biomass waste has gradually attracted attention towards carbon neutralisation and green development. Carbon-based porous material generated from the pyrolysis of biomass under anoxic condition is called biochar (Tu et al. 2019). As an emerging adsorbent, biochar has good applications in the remediation of polluted environments (Fan et al. 2020a, b; Pei et al. 2021; Tomin et al. 2021). However, the adsorption ability of biochar depends on the type of raw material used, pyrolysis condition, pore structure, functional group composition, and surface charge (Ren et al. 2021; Zhang et al. 2017). Conventional biochar often has a negative surface charge, and its adsorption capacity for anionic pollutants, including phosphate, is significantly limited (Ren et al. 2021). Therefore, the adsorption performance of biochar for anionic pollutants can be improved by increasing the density of specific active sites on the biochar surface through rational design and fabrication (Li et al. 2018a). Recently, some biomaterials (chitosan) and metal oxides or hydroxides of Fe, Al, La, Mg, Zr, and Ca have been successfully introduced into biochar, and the resulting metal-biochar engineered composites showed strong affinities towards anionic pollutants present in wastewater (Li et al. 2018a; Zhang and Gao 2013; Imran et al. 2021; Iqbal et al. 2021; Peng et al. 2022; Wang et al. 2022; Zhang et al. 2022). Common methods for preparing the engineered metal-biochar composites include

direct pyrolysis of highly metal-enriched biomass, post-co-deposition of metals with biochar, electric field-assisted biomass pyrolysis, mechanical ball-milling of biochar with metallic minerals, and pyrolysis of biomass impregnated with metal salts (Jung and Ahn 2016; Li et al. 2018a). For example, Yao et al. (2013) prepared Mg-biochar through the direct pyrolysis of highly Mg-enriched tomato tissue for P recovery from an aqueous solution. Wu et al. (2019) mixed the peanut shell biochar with $MgCl_2$ solution, and the co-precipitated MgO biochar was used for the amelioration of polluted soil. Cui et al. (2020) prepared γ-Al_2O_3/Fe_3O_4 biochars for P adsorption using an electrical assistant method. Wang et al. (2018) obtained calcium-containing biochar nanospheres by ball-milling bamboo charcoal with Ca alginate.

Although these metal-biochar composite materials can be effectively obtained using these methods, however, the involvement of unique biomass feedstocks, complex preparation steps, high-cost metal salt reagent application, or extreme process equipment requirements have limited the large-scale production of metal-biochar composites (Li et al. 2018a). To simplify the preparation of metal-biochar and reduce its industrial production cost, it has been suggested that metal-biochar composites can be efficiently prepared through the direct co-pyrolysis of metal-rich minerals and biomass mixtures. For example, Ca-Mg-rich biochar derived from pyrolysing dolomite and sawdust mixture reduced the level of P to < 0.15 mg/L in wastewater (Li et al. 2018b). The nano-MgO biochar composite derived from lotus pods co-pyrolysed with magnesium citrate showed a P capture capacity of 452.75 mg/g (Zhu et al. 2021). In addition, the co-pyrolysis of chicken manure and calcium bentonite mixture produced P-rich slow-release carbon-based fertilisers for usage in soil (Piash et al. 2022). These studies demonstrated that the direct co-pyrolysis of metal-rich minerals with biomass is a feasible low-cost method for producing metal-biochar (An et al. 2020; Deng et al. 2021). Therefore, it was assumed that the co-pyrolysis of Mg-rich magnesite mineral ($MgCO_3$) with biomass could also produce an engineered Mg-rich biochar. However, the feasibility of preparation of Mg-rich biochar from direct co-pyrolysis of magnesite with biomass is seldom confirmed, and the knowledge gap on adsorptive recovery of P from solution and bio-liquid waste water still needs to be addressed.

Thus, in this study, a mixture of magnesite and food waste was co-pyrolysed under oxygen-limited conditions. The prepared engineered biochar composite (MFBC) was characterised and used for P adsorptive recovery. The mechanism influencing factors and mechanism of P recovery were investigated. The potential of MFBC to recover P from bio-liquid wastewater and possibility of using the recovered P-saturated MFBC as a fertiliser in soil were also verified.

2 Materials and methods

2.1 Raw materials

Food waste, mainly composed of rice (~ 95%) and vegetable residues (~ 5%), was obtained from the southern cafeteria of Northwest A&F University, Yangling, China, and dried naturally prior to use. Magnesite (containing approximately 90% $MgCO_3$) was provided by Shandong Duoju Chemical Co., Ltd., Jinan, China. The bio-liquid wastewater (ammonia was stripped in the system before discharging) was obtained from a suburban farm situated near Northwest A&F University and was filtered to remove the suspended matter before use. The basic properties of bio-liquid wastewater included pH (8.76), electrical conductivity (1411 μS/cm), nitrate nitrogen (14.51 mg/L), ammonium nitrogen (1.95 mg/L), and phosphate (98.14 mg P/L). Soil samples were collected from a farmland situated near Yan'an City at a depth of 0–30 cm, were naturally dried and afterwards crushed to a size of < 2 mm prior to use. The basic properties of soil included pH (8.21), organic matter (1.06%), total N (0.357 g/kg), P_2O_5 (1.43 g/kg), K_2O (21.5 g/kg), and available P (10.6 mg/kg). Chinese cabbage seeds were purchased from a local market. Analytically pure chemicals, including KH_2PO_4, $NaHCO_3$, ammonium molybdate tetrahydrate, ascorbic acid, and antimony potassium tartrate, were provided by Guangdong Guanghua Tech. Co. Ltd., Guangzhou, China. Solutions used in all experiments were prepared with distilled water.

2.2 Biochar production and characterisation

Food waste was mixed with magnesite (5:2, w/w) in a porcelain mortar, ground into a homogeneous powder mixture, transferred to a reactor (Bayek MF-1100C-L, China), and heated to 700 °C at a rate of 10 °C/min under anoxic conditions for 2 h. After natural cooling, the obtained solid sample (MFBC) was collected, crushed to a size of < 0.15 mm and kept under vacuum. Food waste biochar (FBC) without magnesite was also produced with the same procedure.

Weight loss associated with the thermal pyrolysis of magnesite and food waste mixture was evaluated using a thermogravimetric analyser (TG/DTG; TGA5500, USA). The thermal analysis was started at 25 °C with a ramping rate of 5 °C/min and reached 1000 °C in a N_2 environment to simulate the pyrolysis process. The ultimate elemental analysis (Elementar vario MACRO cube03030402, Germany) was used to estimate the contents of elemental C, H and N of the samples. The total Mg content was recorded using an

inductively coupled plasma-atomic emission spectrometer (ICP-AES; Agilent 7900, Japan) after the biochar samples were digested using concentrated sulfuric acid and hydrogen peroxide. The specific surface areas (S_{BET}) of the FBC and MFBC were measured using an N_2 adsorption–desorption surface area analyser (ASAP2460 3.01, Micromeritics, USA) at 77 K. The point of zero charge (pHzpc) of the MFBC was measured using the pH determining method recommended elsewhere (Milonjić et al. 2007). The surface micromorphology and distribution of minerals on the biochars were tested using a ZEISS Gemini SEM 300 scanning electron microscope (SEM) equipped with an Oxford energy-dispersive X-ray spectroscopy (EDS) detector. The crystal phases of the biochars were analysed with a Bruker D8 ADVANCE A25 X-ray diffractometer (XRD) at a scanning rate of 10°/min with a 2 theta in the collection range of 20–80°. ThermoScientific K-Alpha X-ray photoelectron spectroscopy (XPS) with Al Kα radiation was performed to observe the chemical state of the elements present on the surface of the sample. A Nicolet iS20 Fourier transform infrared spectroscopy (FT-IR) was used for investigating the functional groups of the biochars in the wavelength range of 400–4000 cm^{-1} after tableting with KBr.

2.3 Adsorption experiment, data analysis and modelling

The P adsorption performances of the biochars were tested using batch experiments. The impacts of solution properties, namely pH (3–11, adjusted with 0.1 mol/L HCl and NaOH solution), concentration (50–1000 mg/L), contact time (0–24 h), ionic strength (0–0.8 mol/L $NaNO_3$ solution), coexisting ions (F^-, Cl^-, NO_3^-, SO_4^{2-}, and CO_3^{2-}), and temperature (288–313 K) on P capture were studied. Specifically, 50 mg biochar was placed in a centrifugal tube containing 50 mL solution (100 mg/L) or bio-liquid wastewater, which was subsequently placed in a shaking platform operating at 180 rpm at 23 °C in the experiment. After shaking, the supernatant was collected and filtered through a 0.22 μm GE nylon filter. The residual P content present in the filtrate was measured using a UV-1280 spectrophotometer. The amount of P adsorbed was quantified using a mass balance. The experimental kinetic data were simulated using a linear pseudo-first-order (Eq. 1), pseudo-second-order (Eq. 2) and an intraparticle diffusion models (Eq. 3); The adsorption isotherm experimental data for P adsorption were fitted using the Langmuir (Eq. 4) and Freundlich models (Eq. 5) (Jung et al. 2019). The thermodynamic characteristics of the adsorptive capture of P by MFBC were analysed using the Van't Hoff (Eq. 6) and Gibbs free energy change (ΔG) equations (Eq. 7) (Zhu and Zhu 2008). All experiments were performed in triplicates.

$$\text{Pseudo-first-order kinetic model, } \ln(q_e - q_t) = \ln q_e - k_1 t \quad (1)$$

$$\text{Pseudo-first-order kinetic model, } t/q_t = 1/\left(k_2 q_e^2\right) + t/q_e \quad (2)$$

$$\text{Intraparticle diffusion model, } q_t = k_i t^{0.5} + C \quad (3)$$

$$\text{Langmuir model, } q_e = K_L Q C_e/(1 + K_L C_e) \quad (4)$$

$$\text{Freundlich model, } q_e = K_f C_e^{1/n} \quad (5)$$

$$\text{Van't Hoff equation, } \ln K_d = \Delta S/T - \Delta H/RT \quad (6)$$

$$\text{Gibbs free energy change equation, } \Delta G = \Delta H - T\Delta S \quad (7)$$

where C_e (mg/L) denotes the P concentration after adsorption and k_1 (1/h) and k_2 (g/mg/h) are the pseudo-first- and pseudo-second-order apparent adsorption rate constants, respectively. k_i and C are the intraparticle diffusion rate constant and intercept, respectively. q_e and q_t (mg P/g) are the P adsorption capacities at equilibrium and time t, respectively. Q (mg P/g) represents the Langmuir capture capacity and K_L denotes the constant of Langmuir model. K_f and n denote the Freundlich model constants. K_d is the equilibrium constant, which is equal to the ratio of q_e to C_e. ΔG (kJ/mol), ΔH (kJ/mol), and ΔS (kJ/mol/K) are the Gibbs free energy, enthalpy, and entropy change, respectively. R is a constant (8.314 J/(mol·K). T (in K) is the temperature.

2.4 Adsorbent reuse

Approximately 100 mg of biochar was mixed with 100 mL phosphate solution (100 mg/L) at 23 °C for overnight. After mixing, the supernatant was collected, filtered and measured. The initial amount of P sorbed (q_i) was calculated. The P-loaded biochar was separated from the solution by centrifugation at 4000 rpm for 15 min. The separated solid was washed with distilled water for 6 times before drying at 100 °C for 2 h. After that, the dry P-loaded biochar (25 mg) was mixed with 25 mL desorption reagent solution (5 mol/L NaOH) for 6 h and the solid was separated from the solution by centrifugation at 4000 rpm for 15 min. The separated solid was washed, dried, and used as adsorbent in the next round of adsorption experiment. The P adsorption efficiency was the ratio of P adsorption amount in each cycle to q_i. The experiments were implemented in triplicates.

2.5 Soil incubation and pot experiments

In the soil incubation test, approximately 20 g FBC, MFBC, and P-loaded MFBC (P-MFBC) were mixed with 200 g soil, respectively. Subsequently, distilled water was added to maintain the moisture at approximately 60% of

the field capacity for a 30-d incubation. A certain number of soil samples were collected at 5 d intervals during this period to measure the available P content in the soil (Olsen and Sommers 1982). The treatment withoutbiochar was used as the control. Each treatment was conducted in triplicates.

In the pot experiment, approximately 3.2 g FBC, MFBC, P-MFBC, and equal amount of phosphorus (KH_2PO_4) were completely mixed in plastic pots with 160 g ofsoil sample, respectively, whereas a treatment without biochar addition (only 160 g soil) was labelled as blank. Distilled water was added to irrigate the soil. After stabilising for 2 weeks, Chinese cabbage (10 seeds) was planted in each pot. During the pot experiment, distilled water was added regularly to keep the soil moist. The height, wet weight, and dry weight (60 °C, 6 h) of the seedlings were measured 12 d after sowing. Each treatment was conducted in triplicates.

3 Result and discussion

3.1 Biochar characterization

As presented in Fig. 1a, the weight loss of 12.33% before reaching the temperature of 220.4 °C was caused by the evaporation of water in the raw materials (Worasuwannarak et al. 2007). The subsequent weight loss (17.95%) was due to the loss of pore water and volatile organic compounds (Martínez et al. 2022). The relatively high weight loss (38.6%) occurring at temperatures above 405 °C was due to the pyrolysis of organic matter and decomposition of magnesite ($MgCO_3 = MgO + CO_2 \uparrow$) (Li et al. 2018b). High-temperature thermal treatment of the biomass would generate porous carbonaceous material, which could be proven by the specific surface area analysis results (Fig. 1b). According to the IUPAC classification, the N_2 adsorption–desorption curve of FBC is a type I isotherm containing microporous structures, while MFBC shows a typical type IV isotherm with an H3 hysteresis loop, reflecting the formation of mesopores. The MFBC showed a lower S_{BET} (298.49 m^2/g) than the FBC (674.41 m^2/g), suggesting the broadening of pore size or blockage of pores in the MFBC. These results were confirmed by SEM analysis (Fig. 1c). The porous FBC sample showed a relatively smooth surface and edge, while the surface of the MFBC sample was uniformly covered by some substances (Fig. 1d). Further EDS analysis revealed that the MFBC surface had a high Mg content distribution (Fig. 1e, f), and this result was also in agreement with the results of the ultimate elemental analysis (Table 1). To confirm the presence of Mg in the MFBC, the samples were further analysed using XRD (Fig. 1g). The FBC showed a typical biochar characteristic peak (Yang et al. 2021). The MFBC showed the typical diffraction peaks of MgO crystals (JCPDS 01-089-7746), including 2 thetas of 36.86° (111), 42.83° (200), 62.17° (220), 74.52° (311), and 78.45° (222) crystal plane diffraction peaks. This observation shows that MgO particles covered the surface of the MFBC, indicating that MFBC was a new MgO-doped biochar composite. Previous experimental results showed that FBC had a significantly lower P capture capability (< 5 mg/g) than the MFBC. Therefore, only MFBC was used for P adsorptive recovery in subsequent experiments.

3.2 Impact of pH of the solution on phosphate adsorption

In the pH range of 3.0–5.0, the P adsorptive amount essentially remained at approximately 95.11 mg P/g, and then slowly decreased to 84.62 mg P/g at pH 11 (Fig. 2a), which may be related to the charge of the biochar and species of phosphate ions present in the system. The pHpzc of MFBC was 11.03, which indicated that the surface of MFBC was positively charged in the experiment condition. In addition, the pH values of the solution after adsorption were stable between 10.66 and 11.07, with all values were higher than the initial pH of the solution (Fig. 2a). The results indicated a strong protonation of MgO particles on the MFBC surface ($\equiv MgO + H_2O \rightarrow \equiv MgOH^+ + OH^-$) during adsorption, which increased the pH (Li et al. 2018b). The positively charged MFBC surface ($\equiv MgOH^+$) showed a strong affinity towards negatively charged phosphate ions, thus maintaining a high P adsorptive amount. In solution, phosphate ions mainly existed as H_3PO_4 and HPO_4^{2-} in the pH range of 2.0–4.3 and as HPO_4^{2-} and PO_4^{3-} in the pH range of 9.3–14 (Fig. 2b). The relatively higher P capture amount in the pH range of 3.0–5.0 was probably due to acidic H_3PO_4 and HPO_4^{2-} favouring the promotion of MgO protonation (Li et al. 2018b). After P adsorption, the final pH of the system remained at approximately 11, indicating that HPO_4^{2-} predominantly interacted with the MFBC surface. Therefore, to balance the capture and economic efficiency, a solution pH 5.0 was selected as the pH value for subsequent experiments.

3.3 Phosphate adsorption isotherm

Figure 3a shows the relationship between the amount of P adsorbed and the contact time. More than 90% of P was captured by MFBC within 0.5 h and the equilibrium was reached within 1 h. The rapid capture of P by MFBC may be ascribed to the strong affinity between the positively charged MFBC surface and negatively charged phosphate ions (Li et al. 2017). The further fitting of the experimental data revealed that the coefficient of determination (R^2) of the pseudo-first-order kinetic model (0.995) was slightly higher than that of the pseudo-second-order kinetic model (0.985) (Table 2). This indicated that physical adsorption

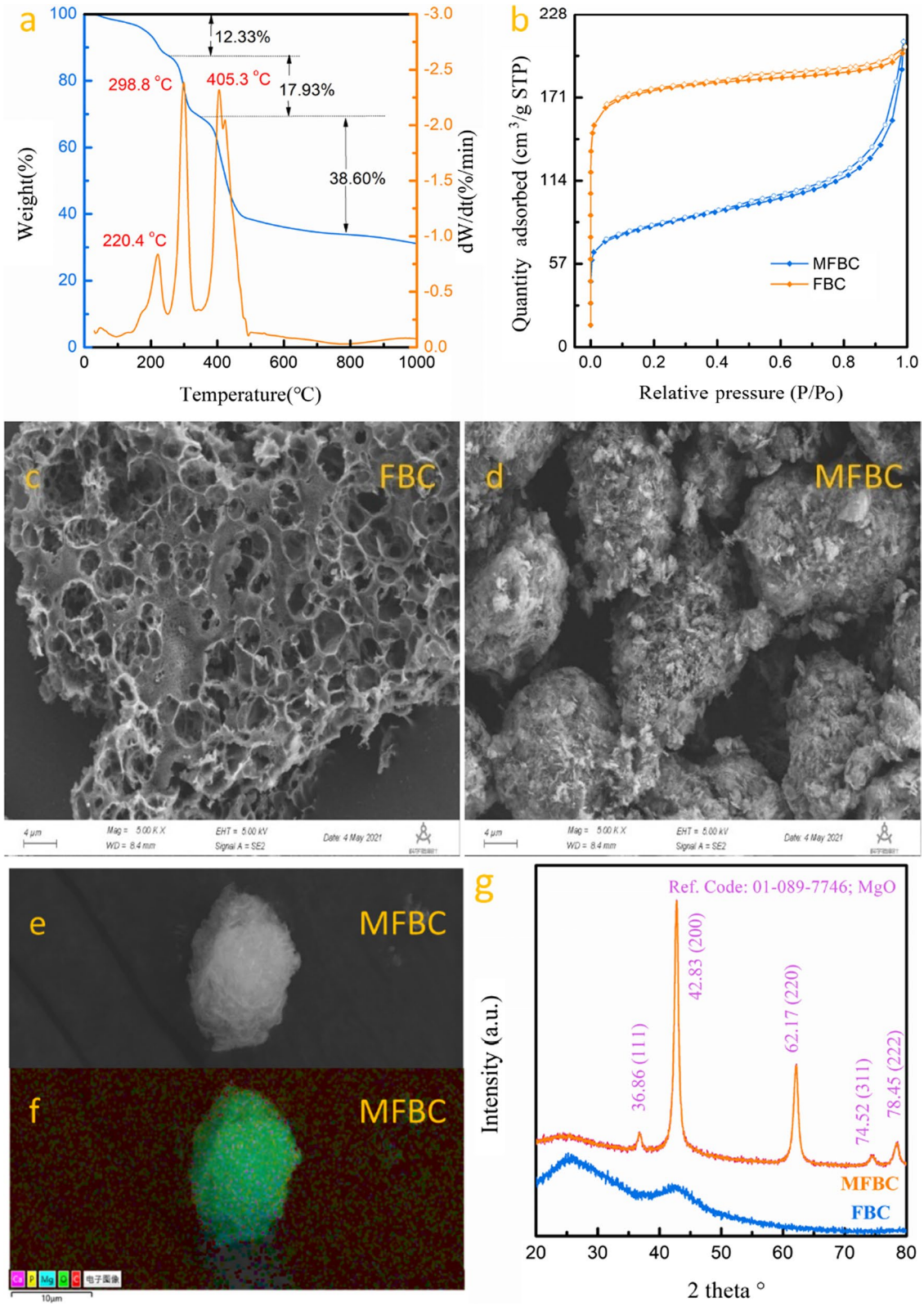

Fig. 1 TG/DTG analysis curve of magnesite and food waste mixture (**a**), BET-specific surface area analysis of biochar (**b**), SEM photographs of FBC (**c**) and MFBC (**d**), selected SEM photographs of MFBC (**e**) and related elemental distribution in EDS-mapping (**f**), and XRD patterns of FBC and MFBC (**g**)

Table 1 Physiochemical properties of the biochars

Samples	C (%)	H (%)	N (%)	Mg (%)	S_{BET} (m^2/g)
FBC	46.37	5.12	2.03	0.87	674.41
MFBC	35.88	5.01	1.89	19.26	298.49

dominated the adsorption process, further demonstrating electrostatic attraction to be the main step in the adsorption of phosphate ions by the MFBC (Wu et al. 2019). To further elaborate the function of the porous structure of MFBC, the experimental data were also simulated using the intraparticle diffusion model (Fig. 3b). The results showed that the line did not pass through the origin of the plot and indicated a multivariate linear relationship. The value of k_{i1} (112.0) was higher than that of k_{i2} (0.043), indicating that membrane diffusion was the rate-determining step, with intraparticle diffusion having a smaller effect on the adsorption rate (Jung et al. 2019).

The P capture amount increased sharply with the increase in P concentration and then gradually reached equilibrium (Fig. 3c). Further fitting of the experimental data showed that the R^2 value of the Langmuir model (0.997) was higher than that of the Freundlich model (0.880) (Table 2), and χ^2 (636.29) of the Langmuir model was smaller than that of the Freundlich model ($\chi^2 = 22{,}485.71$), suggesting that the Langmuir model better described the P adsorptive capture process, implying that the capture of P by the MFBC was a monolayer surface adsorption (Jung et al. 2019). The maximum P capture capacity calculated using the Langmuir model was 523.91 mg/g, which was comparable to that of the most documented material (Table 3).

3.4 Impacts of temperature, ionic strength and coexisting anions on P capture

The process of P adsorptive capture by the MFBC was slightly facilitated by increasing the temperature (Fig. 4a). The P capture amount increased from 96.53 to 100.1 mg/g as the temperature increased from 288 to 308 K. Based on the results shown in Fig. 4b, the calculated thermodynamic parameters were summarised in Table 4. ΔG values were found to be evidently negative, and its absolute values increased with the increase of temperature, indicating that the process was spontaneous (Li et al. 2016a, b). In addition, the positive ΔS showed an increase in the degree of disorder in the interface between MFBC and P. The positive ΔH confirmed that the capture was an endothermic process driven by physicochemical interactions involving electrostatic interactions, rather than a single chemical or physical process (Zhu and Zhu 2008).

The adsorptive capture of P by the MFBC decreased with the increase of ionic strength (Fig. 4c). The P capture amount increased from 99.80 to 77.84 mg/g as the amount of $NaNO_3$ increased from 0 to 0.8 mol/L, which was probably because the high level of NO_3^- ion competed with the phosphate ions for the active sites (Zhu et al. 2021). The results indicated that electrostatic attraction was one of the important mechanisms for P adsorptive capture by the MFBC. In addition, various coexisting anions present in wastewater have been found to usually affect phosphate removal by competing with

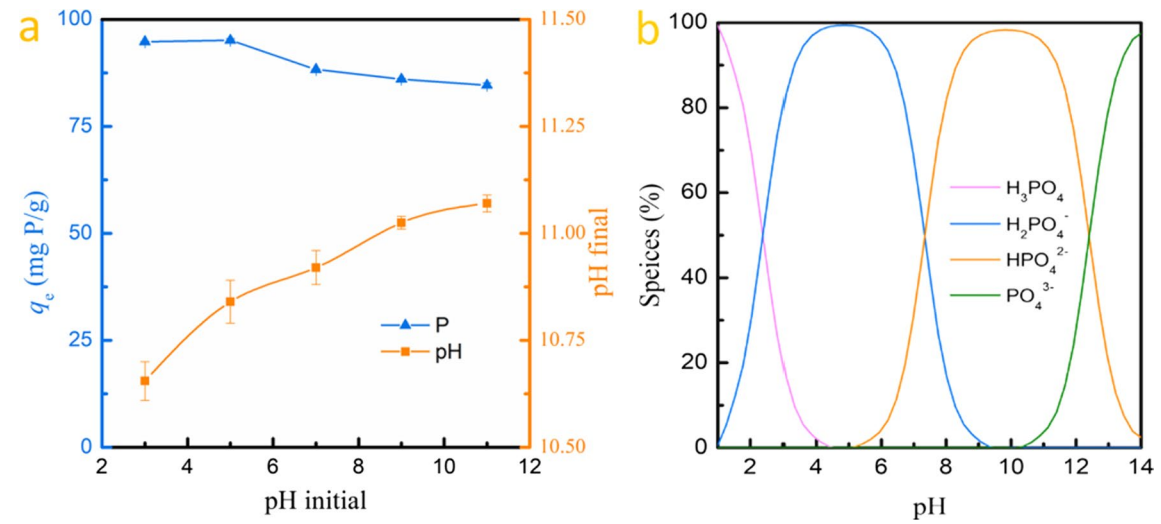

Fig. 2 Effect of solution pH on phosphorus adsorption by MFBC and changes in pH after adsorption (**a**), components distribution of phosphate (100 mg/L) system at different pH conditions (**b**)

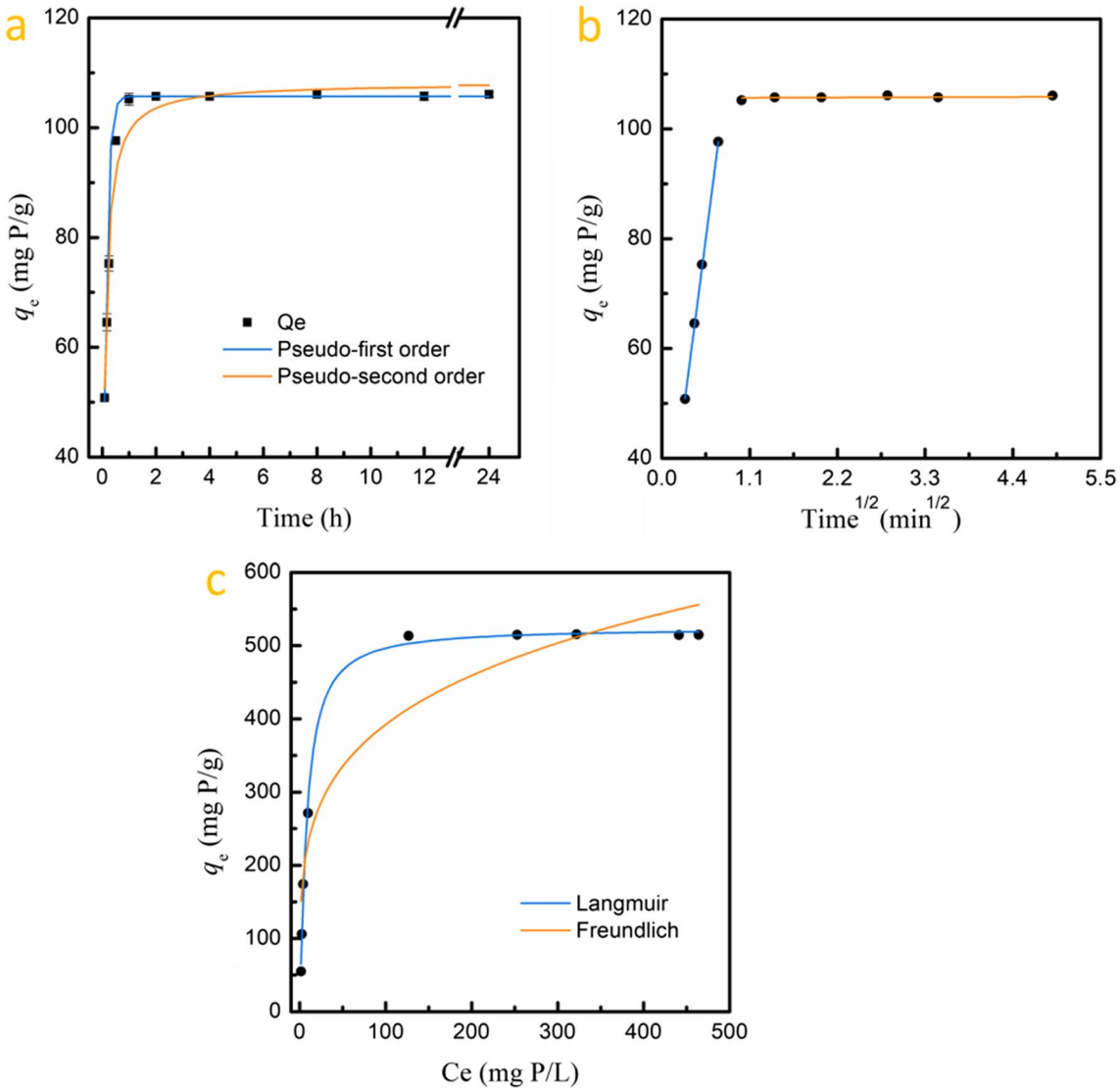

Fig. 3 Effect of contact time on P adsorption by the MFBC and data modelling with **a** the pseudo-first-order and pseudo-second-order kinetic models and **b** intraparticle diffusion model, **c** effect of initial P concentration on the adsorption and experimental data fitting using the adsorption isotherm models

the sorption sites (Jia et al. 2020). The impacts of coexisting anions (Cl^-, F^-, NO_3^-, CO_3^{2-}, and SO_4^{2-}, all in 100 mg/L level, same as phosphate concentration) on P adsorption are shown in Fig. 4d. Among the coexisting anions, F^- ions had a relatively greater inhibitory effect on P adsorption with a 29.28% reduction in the capture amount compared to the control, which was probably due to the strong electronegativity of F^-, which could easily bind to the surface of the protonated adsorbent and occupy the active sites (Cui et al. 2020). CO_3^{2-} ions also had a certain inhibitory effect on P capture, with a 3.63% reduction in the capture amount than that of the control. This may be due to the relatively strong affinity of CO_3^{2-} towards $\equiv MgOH^+$ and the increase in electrostatic repulsion due to the presence of alkaline CO_3^{2-} ions in the system (Jia et al. 2020). In contrast, Cl^-, NO_3^-, and SO_4^{2-} showed no significant effects on P adsorption, which was related to their relatively low affinities (Alhujaily et al. 2020). These results also implied that the adsorptive capture of P by the MFBC

Table 2 Adsorption kinetics and isotherm model parameters obtained from the experiment

Models	Parameters	Values
Pseudo-first-order	$q_{e,cal}$ (mg P/g)	105.7
	k_1 (min^{-1})	7.720
	R^2	0.9951
Pseudo-second-order	$q_{e,cal}$ (mg P/g)	108.1
	k_2 (g/mg min)	0.1043
	R^2	0.985
Intraparticle diffusion	k_{i1} (mg/g $min^{1/2}$)	112.0
	C_1	18.47
	k_{i2} (mg/g $min^{1/2}$)	0.043
	C_2	105.6
Langmuir	Q (mg P/g)	523.9
	K_L (L/mg)	0.0899
	R^2	0.9970
Freundlich	K_f	137.8
	n	4.402
	R^2	0.8802

Table 4 Calculated thermodynamic parameters

Temperature (K)	*Kd* (L/g)	*ΔG* (kJ/mol)	*ΔH* (kJ/mol)	*ΔS* (kJ/mol/K)
288	16.99	−40.69	205.7	0.854
298	19.32	−47.86		
308	22.44	−57.45		

may be controlled by multiple mechanisms (Wu et al. 2022).

The reusability of MFBC is exhibited in Fig. 4e. With the increase of adsorption–desorption cycle number, the P adsorption efficiency of the recycled MFBC dramatically declined from 99.89% in the first cycle to 51.19% in the second cycle, and then gradually decreased to 42.62% after five cycles. These results indicated that the MFBC had strong affinity towards P adsorption, which resulted in the limited reusability for P Adsorption of recycled MFBC.

3.5 Possible capture mechanism

To deduce the mechanism of P adsorptive capture by MFBC, the surface morphology of MFBC (Fig. 1d) was compared with that of P recovered MFBC (P-MFBC) (Fig. 5a, b). It can be clearly seen that some new crystals were produced on the surface of P-MFBC. The EDS spectral analysis further showed that the content of P in the MFBC was significantly low (Fig. 1f), while a large amount of P was present in P-MFBC after P adsorption (Fig. 5c), which also confirmed that MFBC had a strong ability to capture P. To further understand the role of chemical functional groups present in MFBC towards P adsorption, relevant samples were analysed using FT-IR (Fig. 5d). Compared to the MFBC, the Mg-O group signal of P-MFBC centering at 753 cm^{-1}

Table 3 Comparison between the maximum capturing capacities of some biochar adsorbents towards phosphate adsorptive removal

Adsorbents	S_{BET} (m^2/g)	PT (°C)	pH	Dosage (g/L)	Kinetics	Isotherm	Q_{max} (mg/g)	References
MgO-modified biochar	–	600	7.5	4	S	F	18.98	Wu et al. (2019)
Marble waste biochar	92.81	800	8	0.3	S	L	263.17	Deng et al. (2021)
Porous MgO-biochar	253.4–346.5	600	–	0.4	–	L	835	Zhang et al. (2012)
MgO-Co biochar	200	600	5	–	S	L	242	Liu et al. (2021)
$MgCl_2$ modified sugarcane	1440	700	1.9	10	S	Sips	129.79 (P)	Fang et al. (2020)
Paper mill sludge biochar	–	750	–	30	S	L	68.49	Wang et al. (2021)
Calcium-doped biochar	54.40	700	4.5	10	S	L	147 (P)	Antunes et al. (2018)
nZVZ-CMC panda manure biochar	72.96	600	–	2	S	L	154.3	Wang et al. (2021)
Sawdust biomass treated with sludge	988.4	450	–	4	S	R-P	15	Yang et al. (2021)
Core–shell structure γ-Al_2O_3/Fe_3O_4 biochar	233.29	600	5	1	S	L-F	205.7	Cui et al. (2020)
$La(OH)_3$ supported corn straw magnetic biochar	287.40	800	7.0	0.5	AF	L	116.08 (P)	Zhang et al. (2021)
Amino hybrid biopolymer-decorated tea waste magnetic biochar	12.69–13.54	600	4.0	1.0	S	L	53.56–62.06 (P)	Zhang et al. (2022)
Mg/Al-LDHs modified sugarcane leaves biochar	10.17–12.25	550	3.0	2.5	S	L	53.39–81.83 (P)	Li et al. (2016a, b)
MFBC	298.4894	700	5	1	F	L	523.91 (P)	This study

PT, AF, R-P, L, and L-F represent the pyrolysis temperature, Avrami fractional-order model, Redlich-Peterson model, Langmuir model, and-Langmuir–Freundlich model, respectively

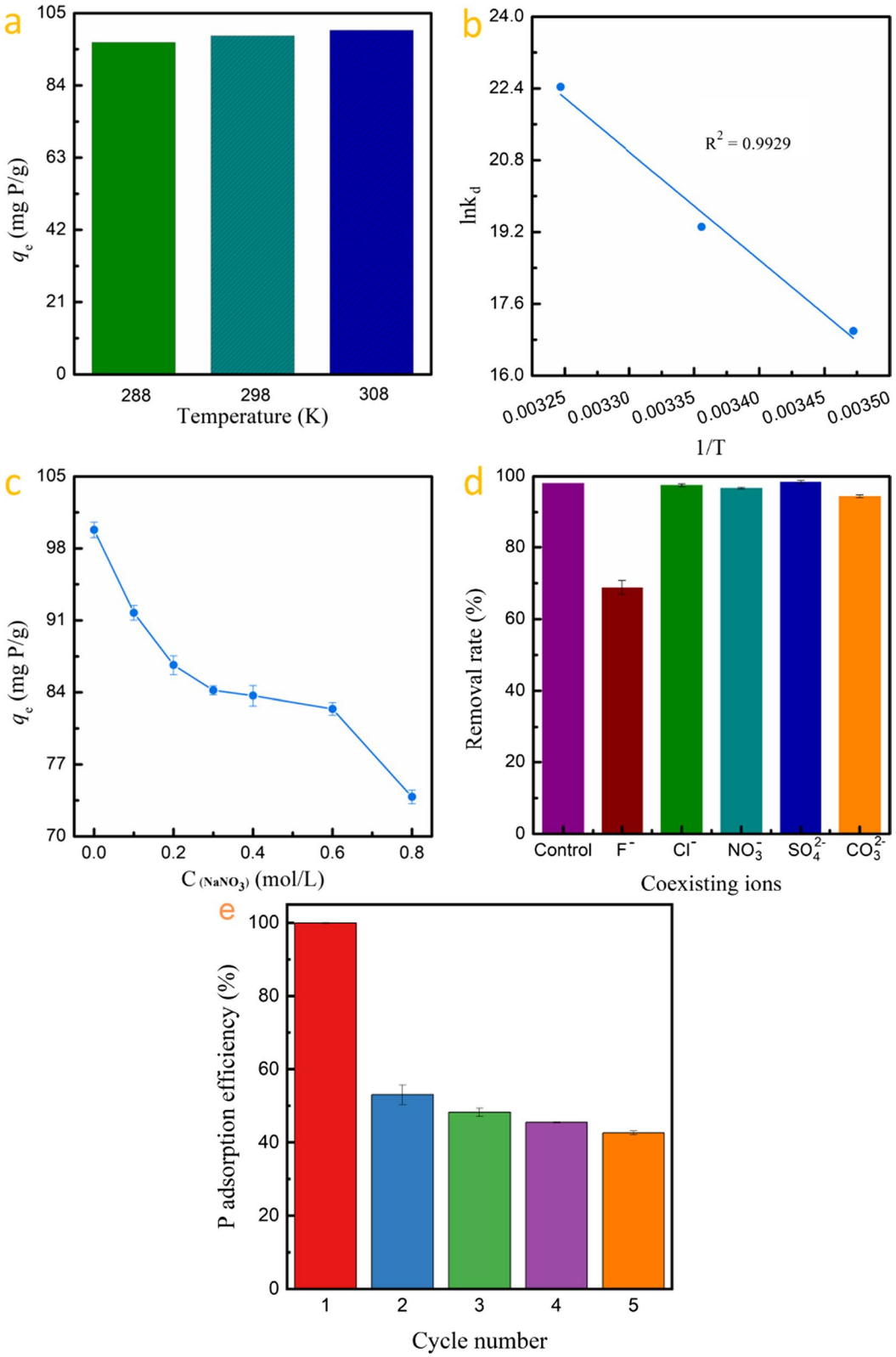

Fig. 4 **a** Effect of temperature on P capture, **b** linear plot of $\ln k_d$ versus $1/T$ for the thermodynamic analysis, effects of **c** ionic strength, **d** coexisting ions on P capture, and adsorbent reuse **e**

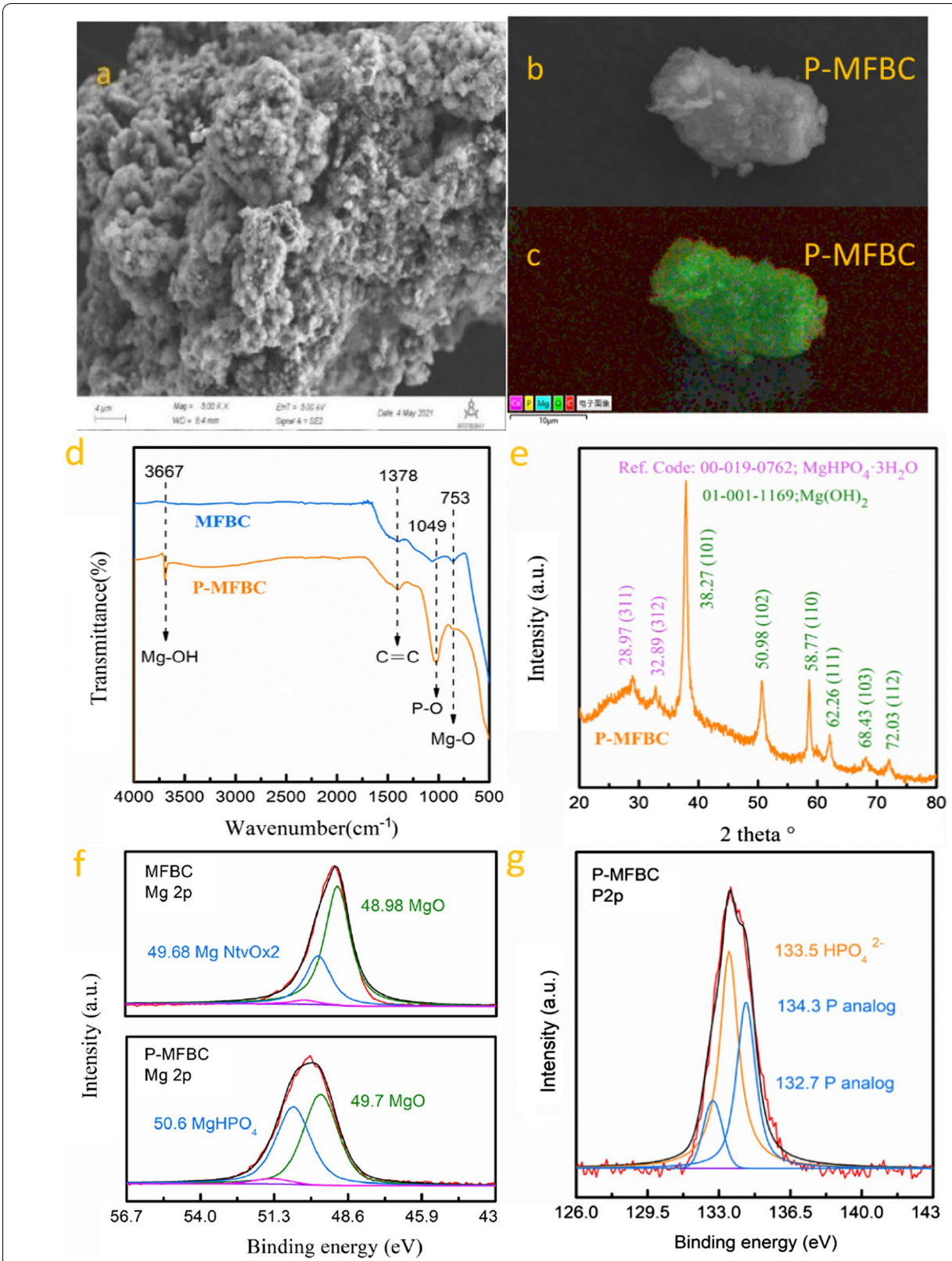

Fig. 5 SEM photographs of P-MFBC (**a**), selected SEM photograph area of P-MFBC (**b**) and related elemental distribution of the EDS-mapping (**c**), FT-IR (**d**) and XRD patterns (**e**) of P-MFBC, high resolution XPS spectra of Mg 1 s (**f**) and P2p of MFBC and P-MFBC samples (**g**)

was found to be weakened (Li et al. 2018b), while the vibration peak of the surface Mg-OH group located at 3667 cm^{-1} (Lichtenberger et al. 2006) was found to have enhanced. These observations proved that MFBC underwent the $\equiv MgO + H_2O \rightarrow \equiv Mg(OH)_2$ and $\equiv MgO + H_2O \rightarrow \equiv MgOH^+ + OH^-$ reactions during P adsorption. Moreover, the appearance of P-O vibration peaking at 1049 cm^{-1} in the P-MFBC sample also indicated the capture of P on MFBC (Li et al. 2018b). Meanwhile, the XRD analysis showed that after P adsorption, the original MgO diffraction peaks in the MFBC disappeared, and some strong peaks of $Mg(OH)_2$ (JCPDS 00-019-0762) and some weak peaks of $MgHPO_4{\cdot}3H_2O$ crystals (JCPDS 01-001-1169) appeared (Fig. 5e). These findings proved the presence of $Mg(OH)_2$ and formation of a small amount of $MgHPO_4{\cdot}3H_2O$ during the P capture process. To fully demonstrate the above-mentioned process, relevant samples were also analysed using XPS. Unlike MFBC, the Mg 2p peak of P-MFBC moved towards higher binding energy (Fig. 5f), implying that MgO interacted with the phosphate ions during the P capture process, which was mainly converted into $Mg(OH)_2$ and $MgHPO_4{\cdot}3H_2O$ with the peak areas accounting for 51.44% and 46.11%, respectively. In addition, the P 2p peak also showed a high proportion of HPO_4^{2-} (50.17%) (Fig. 5g). These results indicated the involvement of surface electrostatic attraction and $MgHPO_4{\cdot}3H_2O$ precipitation during the adsorption of P (HPO_4^{2-}) by the MFBC in the experimental system. Based on the evidences mentioned above, the routes of P capture onto the MFBC can be illustrated as following reactions in Fig. 6.

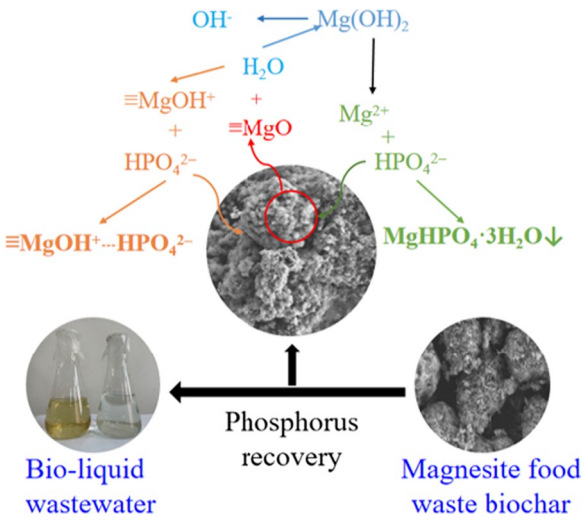

Fig. 6 Possible mechanisms of P recovery using MFBC

$$\equiv MgO + H_2O \rightarrow \equiv MgOH^+ + OH^- \text{(surface protonation)}$$

$$\equiv MgOH^+ + HPO_4^{2-} \rightarrow \equiv MgOH^+ \cdots HPO_4^{2-} \text{(surface electrostatic attraction)}$$

$$\equiv MgO + H_2O \rightarrow \equiv Mg(OH)_2 \rightarrow \equiv Mg^{2+} + 2OH^- \text{(surface hydration and dissolution)}$$

$$\equiv Mg^{2+} + HPO_4^{2-} + 3H_2O \rightarrow MgHPO_4 \cdot 3H_2O \downarrow \text{(surface precipitation)}$$

3.6 Applications of MFBC in bio-liquid wastewater purification and agricultural use

It was found in this study that approximately > 98% of P present in the bio-liquid wastewater was removed by the MFBC within 2 h (Fig. 7a). The experiment also showed that MFBC had the same adsorption ability for organic matter in aquaculture wastewater, which made the wastewater limpid after treatment. Therefore, further experiments should be conducted to understand the adsorption of dissolved organic matter in bio-liquid wastewater using MFBC.

In addition, the P-saturated MFBC (P-MFBC) could act as a fertiliser in soil in view of the relatively high P recovery capability. Therefore, the soil incubation experiment was further conducted, with the releasing of P from P-MFBC into the soil shown in Fig. 7b. P contents remained at 10.61–11.33 mg/kg during 30 d incubation in the soil for the control, FBC, and MFBC groups, while the soil P content increased significantly from 260.5 to 327.7 mg/kg during the first 15 d after P-MFBC was applied to the soil; afterward, the increase slowed down and reached equilibrium. The results demonstrated that P-MFBC had a slow P releasing ability in the soil and had the value of fertiliser used. This was also confirmed in a pot experiment where Chinese cabbage seedlings were grown (Fig. 7c). During the pot experiment, no plant growth was observed

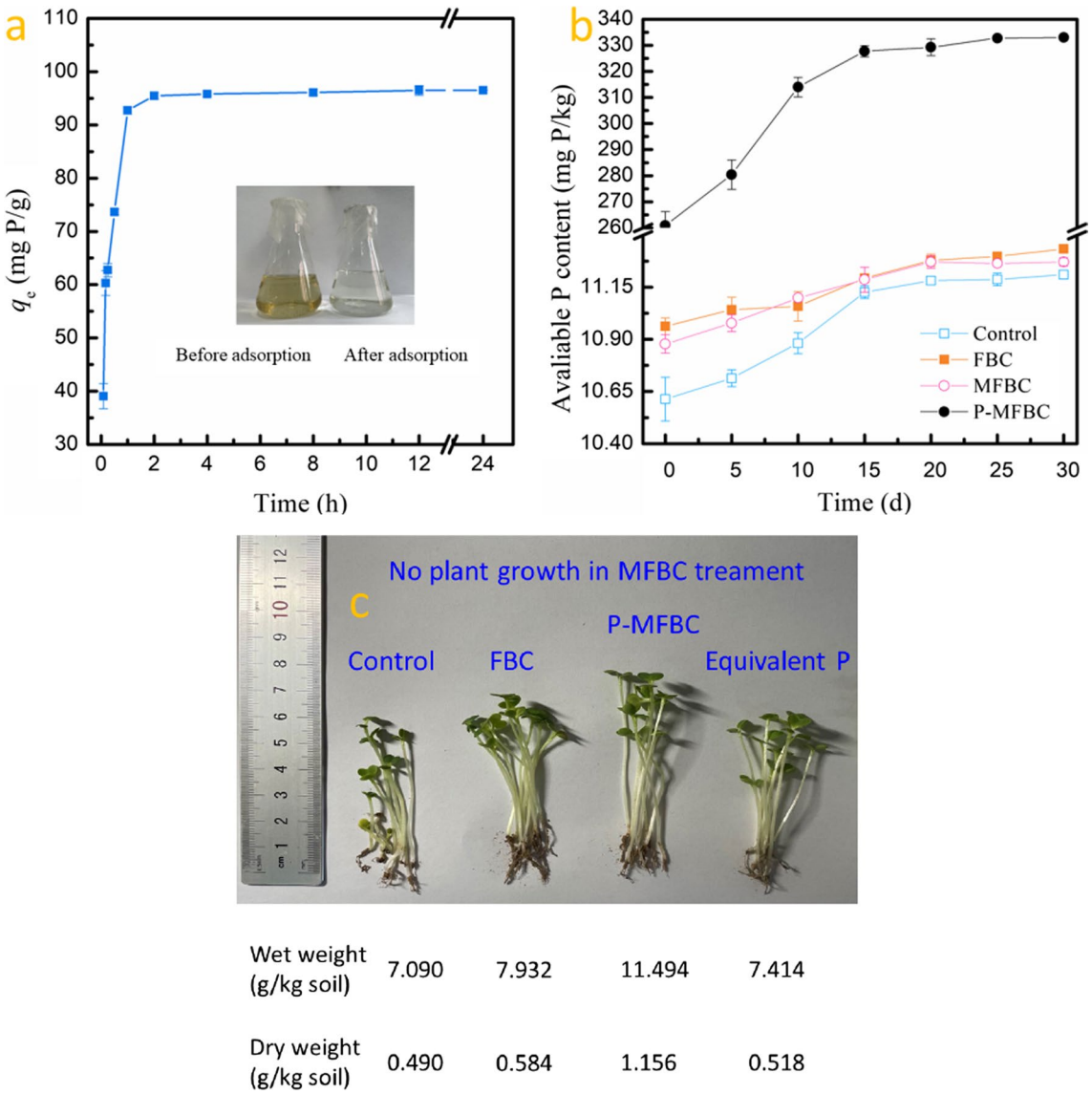

Wet weight (g/kg soil)	7.090	7.932	11.494	7.414
Dry weight (g/kg soil)	0.490	0.584	1.156	0.518

Fig. 7 Effect of contact time on the capture of P from bio-liquid wastewater by the MFBC and model fitting of adsorption kinetics (**a**), release of P in soil (**b**), and potential of P-MFBC to be used as fertiliser for Chinese cabbage growth (**c**)

in the MFBC treatment because of its high alkalinity. Meanwhile, the P-MFBC treatment exhibited relatively higher seedling plant height and biomass than the other treatments, including the control, FBC, and P chemical fertiliser treatments. These results indicated that MFBC was a promising composite having a great potential for recovering of P from bio-liquid wastewater. The recovered P-MFBC was also a substitute for phosphate fertiliser currently in use.

In addition, engineering production and utlisation of MFBC for P recovery from bio-liquid wastewater would promote the recycling use of biowastes in view of sustainable development. Magnesite is an abundant low-cost mineral; food waste is common biowaste that is eligible for government subsidies disposal. The capital cost of MFBC preparation including biomass collection, pretreatment, and pyrolysis could be reckoned at market prices as the method recommended by Huang et al. (2018). For preparing 1 kg MFBC composite, the net cost was 2.10 CNY (Chinese yuan). Using MFBC for recovering P from bio-liquid will generate a P-rich material (P-MFBC, P content 52.39%), which could act as a substitute for phosphate-based fertiliser. Compared with the commercial phosphate fertiliser (Shandong

Xinrui Bio-Tech. Co., Ltd., China) (P content 5.24%; 0.65 CNY/kg), the estimated price of P-MFBC would be approximately 6.50 CNY/kg. Thus, based on the total cost–benefit analysis, the profit of P-MFBC would be 4.40 CNY/kg, suggesting an ideal economic benefit of industrialization.

4 Conclusion

Co-pyrolysis of food waste with magnesite (5:2, w/w) at 700 °C produced MgO-biochar composite (MFBC) successfully. MFBC was an acceptable composite for P recovery from aqueous media. The adsorptive capture of P by MFBC could be simulated using the Langmuir and pseudo-first-order models, with a capture capacity of 523.91 mg/g. The co-existence of F^- and CO_3^{2-} inhibited the P capture. The spontaneous capture of P was achieved via electrostatic attraction and $MgHPO_4$ precipitation, with the electrostatic attraction being predominant. More than 98% of P was adsorptively recovered from the solution and bio-liquid wastewater using MFBC. This study confirmed that direct co-pyrolysis of food waste with magnesite was an economic method for MgO-biochar production; the P-saturated MFBC could be used as a potential fertiliser for the soil. Further experiments could be conducted to declare the practicability of MFBC for recovery of P in engineering practice and to understand the adsorption of dissolved organic matter in bio-liquid wastewater.

Acknowledgements
We are thankful to the finance support from the National Natural Science Foundation of China (31902122, 32172679) and the National College Students Innovation and Entrepreneurship Training Programs of China (2020).

Author contributions
YF: investigation, data curation, methodology, and writing of the original draft. AA: data curation, writing, review, and editing the original draft. YG, PZ, XL and JL: data curation and writing. RL: supervision, conceptualisation, funding acquisition, project administration, review, and editing. YL: data curation. YP, HW, HL and ZZ: Review and editing. JP: conceptualisation, sample characterisation, data analysis, writing, review, and editing the original draft. All authors read and approved the final manuscript.

Funding
The National Natural Science Foundation of China (31902122, 32172679) and the National College Students Innovation and Entrepreneurship Training Programs of China (2020).

Data availability
Data of this work will be made available for reasonable reason.

Declarations

Competing interests
The authors declare that they have no known competing financial interests or personal relationships that could have appeared to influence the work reported in this paper.

Author details
[1]College of Natural Resources and Environment, Northwest A&F University, Yangling, Xianyang 712100, Shaanxi, China. [2]School of Environmental and Municipal Engineering, Shaanxi Key Laboratory of Environmental Engineering, Xi'an University of Architecture and Technology, Xi'an 710055, China. [3]Biochar Engineering Technology Research Center of Guangdong Province, School of Environmental and Chemical Engineering, Foshan University, Foshan 528000, Guangdong, China. [4]Institute of Agricultural Resources and Regional Planning, Chinese Academy of Agricultural Sciences, Beijing 100081, China.

Received: 15 April 2022 Accepted: 29 June 2022
Published online: 24 July 2022

References

Alhujaily A, Mao Y, Zhang J, Ifthikar J, Zhang X, Ma F (2020) Facile fabrication of Mg-Fe-biochar adsorbent derived from spent mushroom waste for phosphate removal. J Taiwan Inst Chem Eng 117:75–85

An X, Wu Z, Yu J, Ge L, Li T, Liu X, Yu B (2020) High-efficiency reclaiming phosphate from an aqueous solution by bentonite modified biochars: a slow release fertilizer with a precise rate regulation. ACS Sustain Chem Eng 8(15):6090–6099

Antunes E, Jacob MV, Brodie G, Philip PA (2018) Isotherms kinetics and mechanism analysis of phosphorus recovery from aqueous solution by calcium-rich biochar produced from biosolids via microwave pyrolysis. J Environ Chem Eng 6(1):395–403

Cui Q, Xu J, Wang W, Tan L, Cui Y, Wang T, Li G, She D, Zheng J (2020) Phosphorus recovery by core-shell γ-Al_2O_3/Fe_3O_4 biochar composite from aqueous phosphate solutions. Sci Total Environ 729:138892

Deng W, Zhang D, Zheng X, Ye X, Niu X, Lin Z, Fu M, Zhou S (2021) Adsorption recovery of phosphate from waste streams by Ca/Mg-biochar synthesis from marble waste calcium-rich sepiolite and bagasse. J Clean Prod 288:125638

Fan D, Mao Y, Xu L, Wang W (2020a) Effects of livestock and poultry breeding pollution on health risks: evidence from a hog breeding case in rural China. Chin J Popul Resour Environ 18(4):342–349

Fan Y, Wang H, Deng L, Wang Y, Kang D, Li C, Chen H (2020b) Enhanced adsorption of Pb(II) by nitrogen and phosphorus co-doped biochar derived from *Camellia oleifera* shells. Environ Res 191:110030

Fang L, Li J, Donatello S, Cheeseman CR, Poon CS, Tsang DCW (2020) Use of Mg/Ca modified biochars to take up phosphorus from acid-extract of incinerated sewage sludge ash (ISSA) for fertilizer application. J Clean Prod 244:118853

Fang Z, Liu F, Li Y, Li B, Yang T, Li R (2021) Influence of microwave-assisted pyrolysis parameters and additives on phosphorus speciation and transformation in phosphorus-enriched biochar derived from municipal sewage sludge. J Clean Prod 287:125550

Huang H, Liang W, Li R, Ali A, Zhang X, Xiao R, Zhang Z, Awasthi MK, Du D, Dang P, Zhang Z (2018) Converting spent battery anode waste into a porous biocomposite with high Pb(II) ion capture capacity from solution. J Clean Prod 184:622–631

Imran M, Iqbal MM, Iqbal J, Shah NS, Khan ZUH, Murtaza B, Amjad M, Ali S, Rizwan M (2021) Synthesis, characterization and application of novel MnO and CuO impregnated biochar composites to sequester arsenic (As) from water: modeling, thermodynamics and reusability. J Hazard Mater 401:123338

Iqbal J, Shah NS, Sayed M, Niazi NK, Imran M, Khan JA, Khan ZUH, Hussien AGS, Polychronopoulou K, Howari F (2021) Nano-zerovalent manganese/biochar composite for the adsorptive and oxidative removal of Congo-red dye from aqueous solutions. J Hazard Mater 403:123854

Jia Z, Zeng W, Xu H, Li S, Peng Y (2020) Adsorption removal and reuse of phosphate from wastewater using a novel adsorbent of lanthanum-modified platanus biochar. Process Saf Environ 140:221–232

Jung K, Ahn K (2016) Fabrication of porosity-enhanced MgO/biochar for removal of phosphate from aqueous solution: application of a novel combined electrochemical modification method. Bioresour Technol 200:1029–1032

Jung K, Lee SY, Choi J, Lee YJ (2019) A facile one-pot hydrothermal synthesis of hydroxyapatite/biochar nanocomposites: adsorption behavior and mechanisms for the removal of copper(II) from aqueous media. Chem Eng J 369:529–541

Li M, Zhang Z, Li R, Wang JJ, Ali A (2016a) Removal of Pb(II) and Cd(II) ions from aqueous solution by thiosemicarbazide modified chitosan. Int J Biol Macromol 86:876–884

Li R, Wang JJ, Zhou B, Awasthi MK, Ali A, Zhang Z, Gaston LA, Lahori AH, Mahar A (2016b) Enhancing phosphate adsorption by Mg/Al layered double hydroxide functionalized biochar with different Mg/Al ratios. Sci Total Environ 559:121–129

Li R, Wang JJ, Zhou B, Zhang Z, Liu S, Lei S, Xiao R (2017) Simultaneous capture removal of phosphate, ammonium and organic substances by MgO impregnated biochar and its potential use in swine wastewater treatment. J Clean Prod 147:96–107

Li R, Wang JJ, Gaston LA, Zhou B, Li M, Xiao R, Wang Q, Zhang Z, Huang H, Liang W, Huang H, Zhang X (2018a) An overview of carbothermal synthesis of metal–biochar composites for the removal of oxyanion contaminants from aqueous solution. Carbon 129:674–687

Li R, Wang JJ, Zhang Z, Awasthi MK, Du D, Dang P, Huang Q, Zhang Y, Wang L (2018b) Recovery of phosphate and dissolved organic matter from aqueous solution using a novel CaO-MgO hybrid carbon composite and its feasibility in phosphorus recycling. Sci Total Environ 642:526–536

Lichtenberger J, Hargroveleak S, Amiridis M (2006) In situ FTIR study of the adsorption and reaction of 2′-hydroxyacetophenone and benzaldehyde on MgO. J Catal 238(1):165–176

Liu X, Wang Y, Smith RL, Fu J, Qi X (2021) High-capacity structured MgO-Co adsorbent for removal of phosphorus from aqueous solutions. Chem Eng J 426:131381

Martínez MG, Couce AA, Dupont C, da Silva PD, Thiéry S, Meyer X, Gourdon C (2022) Torrefaction of cellulose, hemicelluloses and lignin extracted from woody and agricultural biomass in TGA-GC/MS: linking production profiles of volatile species to biomass type and macromolecular composition. Ind Crop Prod 176:114350

Milonjić SK, Čerović LS, Čokeša DM, Zec S (2007) The influence of cationic impurities in silica on its crystallization and point of zero charge. J Colloid Interf Sci 309:155–159

Olsen SR, Sommers LE (1982) Phosphorus methods of soil analysis Part 2. In: Page AL, Miller RH, Keeney DR (eds) Chemical and microbiological properties. Madison, ASA-SSSA, pp 403–430

Pei L, Yang F, Xu X, Nan H, Gui X, Zhao L, Cao X (2021) Further reuse of phosphorus-laden biochar for lead sorption from aqueous solution: isotherm, kinetics, and mechanism. Sci Total Environ 792:148550

Peng Y, Azeem M, Li R, Xing L, Li Y, Zhang Y, Guo Z, Wang Q, Ngo HH, Qu G, Zhang Z (2022) Zirconium hydroxide nanoparticle encapsulated magnetic biochar composite derived from rice residue: application for As(III) and As(V) polluted water purification. J Hazard Mater 423:127081–127081

Piash MI, Iwabuchi K, Itoh T (2022) Synthesizing biochar-based fertilizer with sustained phosphorus and potassium release: co-pyrolysis of nutrient-rich chicken manure and Ca-bentonite. Sci Total Environ 822:153509

Ren L, Li Y, Wang K, Ding K, Sha M, Cao Y, Kong F, Wang S (2021) Recovery of phosphorus from eutrophic water using nano zero-valent iron-modified biochar and its utilization. Chemosphere 284:131391

Tomin O, Vahala R, Yazdani MR (2021) Tailoring metal-impregnated biochars for selective removal of natural organic matter and dissolved phosphorus from the aqueous phase. Micropor Mesopor Mater 328:111499

Tu Z, Ren X, Zhao J, Awasthi MK, Wang Q, Wasthi MK, Zhang Z, Li R (2019) Synergistic effects of biochar/microbial inoculation on the enhancement of pig manure composting. Biochar 1:127–137

Wang B, Gao B, Wan Y (2018) Entrapment of ball-milled biochar in Ca-alginate beads for the removal of aqueous Cd(II). J Ind Eng Chem 61:161–168

Wang M, Hu S, Wang Q, Liang Y, Liu C, Xu H, Ye Q (2021) Enhanced nitrogen and phosphorus adsorption performance and stabilization by novel panda manure biochar modified by CMC stabilized nZVZ composite in aqueous solution: mechanisms and application potential. J Clean Prod 291:125221

Wang F, Li L, Iqbal J, Yang Z, Du Y (2022) Preparation of magnetic chitosan corn straw biochar and its application in adsorption of amaranth dye in aqueous solution. Int J Biol Macromol 199:234–242

Worasuwannarak N, Sonobe T, Tanthapanichakoon W (2007) Pyrolysis behaviors of rice straw, rice husk, and corncob by TG-MS technique. J Anal Appl Pyrol 78:265–271

Wu L, Wei C, Zhang S, Wang Y, Kuzyakov Y, Ding X (2019) MgO-modified biochar increases phosphate retention and rice yields in saline-alkaline soil. J Clean Prod 235:901–909

Wu W, Liu Z, Azeem M, Guo Z, Li R, Li Y, Peng Y, Ali EF, Wang H, Wang S, Rinklebe J, Shaheen S, Zhang Z (2022) Hydroxyapatite tailored hierarchical porous biochar composite immobilized Cd(II) and Pb(II) and mitigated their hazardous effects in contaminated water and soil. J Hazard Mater 437:129330

Xie Z, Yang X, Sun X, Huang L, Li S, Hu Z (2021) Effects of biochar application and irrigation rate on the soil phosphorus leaching risk of fluvisol profiles in open vegetable fields. Sci Total Environ 789:147973

Yang S, Katuwal S, Zheng W, Sharma B, Cooke R (2021) Capture and recover dissolved phosphorous from aqueous solutions by a designer biochar: mechanism and performance insights. Chemosphere 274:129717

Yao Y, Gao B, Chen J, Zhang M, Inyang M, Li Y, Alva A, Yang L (2013) Engineered carbon (biochar) prepared by direct pyrolysis of Mg-accumulated tomato tissues: characterization and phosphate removal potential. Bioresour Technol 138:8–13

Zhang M, Gao B (2013) Removal of arsenic, methylene blue, and phosphate by biochar/AlOOH nanocomposite. Chem Eng J 226:286–292

Zhang M, Gao B, Yao Y, Xue Y, Inyang M (2012) Synthesis of porous MgO-biochar nanocomposites for removal of phosphate and nitrate from aqueous solutions. Chem Eng J 210:26-32

Zhang X, Gao B, Zheng Y, Hu X, Creamer AE, Annable MD, Li Y (2017) Biochar for volatile organic compound (VOC) removal: sorption performance and governing mechanisms. Bioresour Technol 245:606–614

Zhang Y, Akindolie MS, Tian X, Wu B, Hu Q, Jiang Z, Wang L, Tao Y, Cao B, Qu J (2021) Enhanced phosphate scavenging with effective recovery by magnetic porous biochar supported $La(OH)_3$: kinetics, isotherms, mechanisms and applications for water and real wastewater. Bioresour Technol 319:124232

Zhang Y, Shi G, Wu W, Ali A, Wang H, Wang Q, Xu Z, Qi W, Li R, Zhang Z (2022) Magnetic biochar composite decorated with amino-containing biopolymer for phosphorus recovery from swine wastewater. Colloid Surf A 634:127980

Zhu R, Zhu L (2008) Thermodynamics of naphthalene sorption to organoclays: Role of surfactant packing density. J Colloid Interf Sci 322(1):27–32

Zhu D, Yang H, Chen X, Chen W, Cai N, Chen Y, Zhang S, Chen H (2021) Temperature-dependent magnesium citrate modified formation of MgO nanoparticles biochar composites with efficient phosphate removal. Chemosphere 274:129904